Research Square

Preprints are preliminary reports that have not undergone peer review.
They should not be considered conclusive, used to inform clinical practice,
or referenced by the media as validated information.

Microbial strategy shifts drive seasonal reversal of litter decomposition in drylands across hydrothermal thresholds

Meiqi Li
Xinjiang Institute of Ecology and Geography
Yalan Liu
Xinjiang Institute of Ecology and Geography
Peng Wang
Xinjiang Institute of Ecology and Geography
Xiangyi Li
lixy@ms.xjb.ac.cn

Xinjiang Institute of Ecology and Geography

Research Article

Keywords: Litter decomposition, Seasonal metabolic bottleneck, Microbial carbon use efficiency, Enzyme stoichiometry, Extreme arid zone

Posted Date: November 12th, 2026

DOI: https://doi.org/10.21203/rs.3.rs-11537873/v1

License: This work is licensed under a Creative Commons Attribution 4.0 International License.
Read Full License

Additional Declarations: No competing interests reported.

Microbial strategy shifts drive seasonal reversal of litter decomposition in drylands across hydrothermal thresholds

Meiqi Li[a, b, c, d], Yalan Liu[a, b, c, d], Peng Wang[a, b, c, d], Xiangyi Li[a, b, c, d]

[a]Xinjiang Key Laboratory of Desert Plant Root Ecology and Vegetation Restoration, Xinjiang Institute of Ecology and Geography, Chinese Academy of Sciences, Urumqi 830011, China

[b]State Key Laboratory of Desert and Oasis Ecology, Xinjiang Institute of Ecology and Geography, Chinese Academy of Sciences, Urumqi, 830011

[c]National Field Scientific Observation and Experimental Station of Cele Desert Grassland Ecosystem, Cele 848300, Xinjiang, China

[d]University of Chinese Academy of Sciences, Beijing 100049

Corresponding authors' address: Xinjiang Institute of Ecology and Geography, Chinese Academy of Sciences, Urumqi, 830011, China. *E-mail*: lixy@ms.xjb.ac.cn (X. Li)

Abstract: Litter decomposition in arid regions is driven by seasonal microbial carbon (C) allocation trade-offs and enzymatic stoichiometric strategies, yet synergistic regulation by precipitation and phosphorus (P) remains unclear. This 720-day study revealed the microbial mechanisms linking hydrothermal thresholds to seasonal decomposition asynchrony. Mass loss (31.07%–57.06%) depended strongly on the brief summer hydrothermal window. In summer, opportunistic taxa (e.g., *Firmicutes*, *Bacillus*) were rapidly enriched, but structural equation modeling (SEM) revealed that the true functional hubs driving increases in *β*-1,4-glucosidase (BG), leucine aminopeptidase (LAP), and C use efficiency (CUE) were *Proteobacteria* and bacterial Shannon diversity. These taxa adopted a "get-then-grow" strategy, accelerating decomposition and indicating a decoupling of community abundance from functional contribution. In winter, low temperature coupled with physiological drought triggered a widespread regulatory constraint. Dominant taxa shifted to stress-tolerant groups, including *Actinobacteria*, *Basidiomycota* (e.g., *Coprinellus*, *Schizophyllum*), and *Psychrophilic yeasts* (e.g., *Mrakia*, *Filobasidium*). *Actinobacteria* became the functional hub driving a recalcitrant C mining strategy centered on polyphenol oxidase (PPO), with CUE turning negative and assimilated C shifting to intracellular storage. Compared to single-species litter, mixed-species litter decomposition exhibited a significant seasonal reversal. In summer, stoichiometric complementarity produced a synergistic effect (relative mixture effect (RME) > 8%). In winter, mixed-species litter sustained functional redundancy via enrichment of specific taxa (e.g., *Ornithinimicrobium*, *Balneimonas*), yet high lignin content created a metabolic bottleneck. The WMP and WHP treatments shifted to significant antagonism (RME = −12.48% and −7.75%, respectively). Parameterizing arid-region C cycling requires incorporating seasonal CUE, enzyme trade-offs, and functional assembly into biogeochemical models.

Keywords: Litter decomposition; Seasonal metabolic bottleneck ; Microbial carbon use efficiency; Enzyme stoichiometry; Extreme arid zone

1 Introduction

Litter decomposition is a core biogeochemical process regulating soil organic C accumulation and nutrient cycling in arid and semi-arid regions (Parton et al., 2007; Day et al., 2022; Li et al., 2026). In extremely arid areas, decomposition rates are shaped by intermittent precipitation pulses and intense ultraviolet (UV) radiation (Joly et al., 2017; Austin & Ballaré, 2024; Yang et al., 2024a). However, a more fundamental limitation arises from the seasonal asynchrony of precipitation and temperature. A brief summer hydrothermal window contrasts sharply with the prolonged low-temperature drought of winter (Qu et al., 2024; Liu et al., 2025). Cold winters not only reduce microbial cell membrane fluidity and disrupt osmotic homeostasis but also induce a "physiological drought" analogous to water stress (Schimel et al., 2007; Jefferies et al., 2010). Although soil moisture is not absolutely limiting, low temperatures inhibit liquid-phase diffusion and biochemical reaction rates. This substantially reduces moisture actually available to microorganisms (Jefferies et al., 2010) and continuously suppresses metabolic activity during the non-growing season (Imminger et al., 2024). Under global change, increasing uncertainty in precipitation patterns and rising atmospheric P deposition further strengthen nonlinear interactions among precipitation, temperature, and nutrients (Liu et al., 2024). Consequently, traditional decomposition models based on annual climate parameters fail to accurately depict soil C turnover processes constrained by hydrothermal thresholds (Joly et al., 2017).

Classical decomposition theory focuses primarily on the direct regulatory effects of substrate quality and macroclimatic factors (Olson, 1963; Parton et al., 2007). However, in extremely arid regions with severely limited water availability, litter decomposition is essentially driven by a microbial resource allocation strategy for survival. According to the resource conservation hypothesis (Allison & Vitousek, 2005; Sinsabaugh et al., 2009), microorganisms can dynamically adjust extracellular enzyme stoichiometry to cope with imbalances in environmental C:N:P (Gong et al., 2023; Sun et al., 2024). Exogenous P addition alleviates microbial P limitation and accelerates decomposition (Shi et al., 2021; Chen & Xiao, 2023). Yet its effects exhibit marked seasonal asymmetry. During warm, wet periods, enhanced P availability promotes metabolism and enzyme synthesis by increasing microbial CUE (Manzoni et al., 2012; Bolscher et al., 2024). Under cold or drought stress, this pathway is largely blocked due to energy metabolism limitations, inhibited ribosome synthesis, and disrupted post-translational modifications of enzyme proteins (Dijkstra et al., 2011; Cui et al., 2024). Although nutrient additions are effective only under suitable hydrothermal conditions (Gong et al., 2022; Lian et al., 2025), how hydrothermal thresholds reshape microbial physiological trade-offs and enzymatic stoichiometric investment remains unintegrated into arid-region decomposition theory.

Mixed-species litter decomposition often exhibits non-additive effects that deviate

from the expected sum of single-species litter decomposition rates (Gartner & Cardon, 2004; Hättenschwiler et al., 2005; Berglund et al., 2012). Traditional explanations attribute this pattern mainly to physical contact promotion and leaching of allelochemicals (Zhou et al., 2020). However, in arid regions, substrate stoichiometric complementarity is easily masked by strong seasonal environmental filtering (Li et al., 2022; Liu et al., 2025). The synergistic mixing effects observed in temperate regions (Bai et al., 2026) may become neutral or antagonistic in resource-limited environments (Zhou et al., 2024). During summer with favorable hydrothermal conditions, functional complementarity of nutrients and C sources among different litter components can maintain synergistic decomposition (Gartner & Cardon, 2004; Xiao & Chen, 2021). In winter, low-temperature-induced physiological drought renders high-lignin components a "metabolic bottleneck", which not only limits C acquisition efficiency but also exacerbates the inhibition of extracellular enzyme kinetics and turnover delays (Schimel et al., 2007; Sun et al., 2024). This seasonal reversal depends not only on initial litter chemical properties but is also closely linked to the functional strategy shift of microbial groups from hydrolase- to oxidase-dominated processes at the seasonal scale (Sinsabaugh et al., 2009; Lian et al., 2025). However, the seasonal succession patterns of microbial communities, their co-occurrence network structures, and their responses to precipitation-P interactions remain unclear. In particular, there is a lack of systematic analysis regarding the coupled chain of "initial stoichiometry – community assembly – enzymatic stoichiometric investment – decomposition stage transition".

Based on these research gaps, we propose a core hypothesis: the seasonal dynamics of litter decomposition in extremely arid regions are governed by a cascade of "hydrothermal threshold → microbial physiological trade-offs → community assembly and enzymatic stoichiometric investment". Specifically, (i) P addition exerts positive effects only during the summer hydrothermal window by increasing CUE and enzyme synthesis efficiency; physiological drought in winter markedly suppresses this pathway. (ii) Mixed-species litter decomposition shows seasonal reversals: some treatments exhibit synergy in summer, whereas in winter, exacerbated metabolic bottlenecks and declined hydrolase function lead to antagonism. (iii) Initial litter stoichiometric characteristics are closely associated with the temporal succession of microbial communities and their seasonal shifts in co-occurrence network topology, which collectively regulate the functional ratio of hydrolases to oxidases, thereby influencing the seasonal trajectory of decomposition. To test these hypotheses, we conducted field experiments in an extremely arid region using two dominant desert shrubs, *Alhagi camelorum* Fisch. and *Karelinia caspia*, as test species. We established precipitation gradients and P addition treatments, monitored decomposition for 720 days, and measured soil physicochemical properties, microbial biomass, CUE, extracellular enzyme activities, and bacterial and fungal community composition via high-throughput sequencing. Multi-scale analyses included redundancy analysis (RDA), random forest regression, and structural equation modeling. This study elucidates the mechanisms by which microbial communities regulate the soil C cycle

through physiological and ecological functions. The findings provide empirical evidence and parameterization support for incorporating seasonal microbial functional parameters into biogeochemical models for arid regions.

2 Materials and methods

2.1 Study site

The field experiment was conducted at the Cele Desert Grassland Ecosystem National Field Scientific Observation and Research Station (80°43′45″E, 37°00′57″N), Xinjiang, China, which is located in the oasis–desert ecotone along the southern margin of the Tarim Basin. This region has a typical warm-temperate continental extremely arid climate, with an annual mean precipitation of only 42.6 mm (the recent maximum is ~100 mm) and annual evaporation exceeding 2600 mm. The mean annual temperature is 12.8 °C, ranging from -22.3 to 45.7 °C. The meteorological background for the study period is presented in Fig. S1. The soil is a mobile aeolian sandy soil with low organic matter content and available P (< 5 mg/kg). Vegetation is dominated by desert shrubs, including *Alhagi camelorum* Fisch., *Karelinia caspia*, and *Populus euphratica*. These species form a typical desert vegetation community in arid landscapes (Gao et al., 2024; Li et al., 2026).

2.2 Experimental design

The experiment was initiated on 7 December 2023, using a randomized block design. The full experimental design consisted of 16 treatment combinations (2 litter types × 8 precipitation and P treatments) with three replicates, totaling 48 plots (4 m × 4 m each, with 1 m spacing). Two precipitation levels were applied: ambient precipitation (CK) and a 50% increase in maximum ambient precipitation (W, approximately +50 mm yr^{-1}). Four P addition levels were used: 0, 1, 2.5, and 5 g P m^{-2} yr^{-1} (designated as P0, LP, MP, and HP, respectively). Consequently, the 8 precipitation–P treatments were CK (P0 + ambient precipitation), W (P0 + W), LP, MP, HP, WLP, WMP, and WHP. Precipitation and P addition levels were set based on the local maximum precipitation and mean annual atmospheric P deposition (Gao et al., 2025; Liu et al., 2025; Li et al., 2026). The 0 g P m^{-2} treatment represented background conditions, whereas the 1 g P m^{-2} treatment represented a moderate enrichment (~12–20× the regional atmospheric P deposition background of ~0.05–0.08 g P m^{-2} yr^{-1} in the southern Taklamakan Desert); the 2.5 and 5 g P m^{-2} treatments represented an anthropogenic P-enrichment disturbance scenario (Tipping et al., 2014; Pan et al., 2021). Precipitation addition was distributed during the growing season (May–September) as five equal 10-mm events (equivalent to ~160 L per plot per event) using a portable sprinkler (10 mm h^{-1}) in the early morning. P was applied as a $NaH_2PO_4 \cdot 2H_2O$ solution (0, 8.0, 20.0, and 40.0 g P L^{-1} stock solutions; 2 L $plot^{-1}$ yr^{-1}) in two equal doses on 10 May and 5 July, with the spraying order randomized daily. Detailed rationale and operational procedures are provided in Appendix S1.

2.3 Sample collection and processing

Two dominant species, *Alhagi camelorum* Fisch. (Fabaceae) and *Karelinia caspia* (Asteraceae), were selected as litter sources for their contrasting initial chemistry (Fan et al., 2021). Mixed-species litter was prepared at a 1:1 mass ratio. Freshly fallen leaves collected in early December 2023 were air-dried and oven-dried at 75 °C for 48 h. Approximately 10 g of leaves were placed into 10 × 10 cm nylon litterbags (1-mm mesh) and weighed to the nearest 0.01 g. Initial C, N, P, cellulose, and lignin were determined from three subsamples (Table S1). A total of 240 litterbags were prepared (2 litter types × 8 treatments × 3 replicates × 5 sampling dates). On 7 December 2023, litterbags were randomly placed on the soil surface and secured with 10 cm stainless steel nails. Plots were inspected biweekly and weeded monthly within 10 cm of the bags. Samples were collected on days 90, 180, 360, 540, and 720 (48 bags per date). Rodent density was low and no visible animal disturbance occurred. The 1-mm mesh excludes macrofauna but permits microbial and microarthropod access. Because bags were surface-placed, UV-B was partially intercepted and photochemical oxidation was not quantified; thus measured mass loss predominantly reflects microbial decomposition, excluding macrofaunal fragmentation and photodegradation.

2.4 Sample analysis

2.4.1 Litter and soil chemical properties, and microbial biomass C, N, and P

Litter samples were placed in an ice box (< 4 °C) and transported to the laboratory within 6 h. Attached sand particles were gently brushed off with a soft brush, and the samples were oven-dried at 75 °C to constant weight for determination of mass remaining. Subsamples for C, N, P, and lignin analyses were freeze-dried to constant weight, ground using a ball mill, passed through a 0.15 mm sieve, sealed in polyethylene bags, and stored at −20 °C in the dark (Liu et al., 2025). Total carbon (TC) and total nitrogen (TN) contents of the litter were determined using a CN elemental analyzer (Elementar, Hanau, Germany) (Shi et al., 2021). Total phosphorus (TP) was measured by the molybdenum–antimony colorimetric method. Lignin content was determined using a fiber analyzer (FOSS, Hilleroed, Denmark) combined with the modified Klason method and the acid detergent lignin (ADL) method (Van Soest, 1967; Hou et al., 2021).

Litterbags retrieved at 540 d (summer) and 720 d (winter) were used to collect soil attached to the litter surface for analyses of soil physicochemical properties and microbial biomass. Soil pH was measured with a calibrated pH meter. SOC, TN, and TP were determined using a CHNS elemental analyzer. Available phosphorus (AP) was measured by the molybdenum blue colorimetric method. Nitrate (NO_3^--N) and ammonium (NH_4^+-N) were determined using a flow analyzer. Microbial biomass carbon, nitrogen, and phosphorus (MBC, MBN, MBP) were measured by the

chloroform fumigation–K_2SO_4 extraction method (Jenkinson & Powlson, 1976; Brookes et al., 1985; Vance et al., 1987). Detailed procedures, extraction conditions, and correction coefficients are provided in Appendix S2.

2.4.2 Microbial community analysis

Bacterial 16S rRNA gene V3–V4 regions (338F: 5′-ACTCCTACGGGAGGCAGCAG-3′; 806R: 5′-GGACTACHVGGGTWTCTAAT-3′) and fungal ITS1 regions (ITS5: 5′-GGAAGTAAAAGTCGTAACAAGG-3′; ITS2: 5′-GCTGCGTTCTTCATCGATGC-3′) were amplified. PCR reactions were performed in a 25-μL mixture containing standard Taq Master Mix, 1 μL of each primer (10 μM), 1 μL of template DNA, and ddH_2O. Three independent PCR technical replicates were performed per sample. Amplification products were verified by 1.5% agarose gel electrophoresis and purified using the UltraClean® PCR Clean-Up Kit (Mo Bio Laboratories) (Zheng et al., 2021), after which the purified amplicons were pooled at equimolar ratios. The PCR program was as follows: initial denaturation at 94 °C for 5 min; 35 cycles of denaturation at 94 °C for 45 s, annealing at 50 °C for 45 s, and extension at 72 °C for 90 s; and a final extension at 72 °C for 10 min. The pooled amplicons were sequenced on an Illumina MiSeq platform (paired-end 250 bp). Raw paired-end reads were quality-filtered, denoised, and inferred into exact amplicon sequence variants (ASVs) using the DADA2 pipeline (Callahan et al., 2016). Briefly, primer sequences were removed with cutadapt, after which reads were truncated according to the per-sample quality distribution (typical truncLen of approximately 240/200 bp for forward/reverse reads), with filtering parameters set to maxN = 0, maxEE = c (2, 2), and truncQ = 2. Chimeras were removed using the de novo method. Bacterial and fungal ASVs were taxonomically annotated using naive Bayes classifiers trained on the SILVA 138.1 (Quast et al., 2013) and UNITE 9 (Nilsson et al., 2019) databases, respectively. For fungal communities, non-fungal sequences (*Arthropoda*, *Anthophyta*) were removed from the ITS ASV table before calculating relative abundances at the phylum and genus levels. Bacterial relative abundances were derived directly from the 16S ASV table.

2.4.3 Soil extracellular enzyme assays

Soil extracellular enzyme activities were measured using 96-well microplate fluorometric (hydrolytic) and colorimetric (oxidative) assays (Saiya-Cork et al., 2002; DeForest, 2009). Target enzymes included β-1,4-glucosidase (BG), leucine aminopeptidase (LAP), alkaline phosphatase (ALP), polyphenol oxidase (PPO), and peroxidase (POD, with H_2O_2). Briefly, 1 g fresh soil was suspended in 125 mL buffer (50 mM sodium acetate pH 5.0 for BG, LAP, PPO, POD; 50 mM Tris-HCl pH 8.0 for ALP), shaken 1 min, settled 5 min, and 200 μL supernatant was mixed with 50 μL substrate. Hydrolytic enzymes (BG, LAP, ALP) were measured fluorometrically (Ex 365 / Em 450 nm); oxidative enzymes (PPO, POD) were measured colorimetrically

(absorbance 470 nm). Hydrolytic plates were incubated at 20 °C in darkness for 4 h; POD was incubated for 5 min and PPO for 5 h. Fluorescence or absorbance was measured using a Synergy H1 microplate reader, and enzyme activities were calculated from standard curves after blank correction and expressed as nmol g^{-1} h^{-1}. Measured enzyme activities are proxies for microbial functional potential, not in situ decomposition. Environmental constraints suppress actual efficiency without reducing enzyme abundance, decoupling potential activity from mass loss (Nannipieri et al., 2018).

2.5 Data analysis

All statistical analyses and graphical visualizations were performed using R 4.1.0. Calculation formulas for all indices, parameter sensitivity analyses, network construction details, and supplementary data are provided in Appendices S3–S7, Tables S1–S12, and Fig. S3–S10. One-way ANOVA combined with Tukey's post hoc test was used to compare differences among treatments in decomposition rate (k), soil physicochemical properties, microbial biomass, extracellular enzyme activities and their stoichiometric ratios, nutrient use efficiencies, and α-diversity indices. Linear mixed-effects models (LMMs; lme4 package) were used to evaluate the effects of precipitation, P addition, sampling time, and their interactions on each variable, and to separately assess the interactive effects of precipitation, P addition, and litter type in summer and winter; block was treated as a random effect and all other factors as fixed effects (Wang et al., 2020). For relative mixture effect (RME), season was treated as a fixed factor and treatment as a random effect in the LMMs.

Petal diagrams were constructed from a presence–absence matrix to display shared and unique ASV counts among treatments. Based on ASV relative abundances, the relative abundance distributions of bacterial and fungal communities were calculated at the phylum and genus levels, with genus-level data presented as heatmaps combined with hierarchical clustering. Bacterial and fungal α-diversity was visualized using boxplots. In addition, PCoA was performed based on the Bray–Curtis dissimilarity matrix, and PERMANOVA (999 permutations) was used to test for differences among groups (Wahdan et al., 2023; Gao et al., 2024). Redundancy analysis (RDA; vegan package) was conducted with prevalence-filtered, non-rarefied ASV abundance tables as the response variable and litter mass loss, soil physicochemical properties, microbial biomass, enzyme activities, and nutrient parameters as explanatory variables. Mantel tests combined with Spearman correlation analysis were used to examine the relationships among litter mass loss, soil physicochemical properties, microbial biomass, enzyme activities, and microbial community characteristics. Co-occurrence networks were built on non-rarefied ASV tables after filtering for prevalence (present in ≥ 20% of samples within each group) and mean relative abundance (≥ 0.01%), using Spearman correlations ($|r| > 0.7$, FDR < 0.01). Topological parameters followed Zheng et al. (2021) and Jameson et al. (2023), with complexity as mean standardized indices; visualized in Gephi 1.0. Edges

indicate statistical associations, not biological interactions. LEfSe (LDA > 2.0, $p < 0.05$) identified biomarkers; SIMPER quantified genus-level community differentiation. Random forest (exploratory) built four models to rank predictor importance for mass loss. Predictors were VIF-screened (> 5 excluded); models used ntree = 500, nodesize = 5, 5-fold CV (CV R^2, RMSE), with %IncMSE importance. Results serve hypothesis generation only. PiecewiseSEM tested direct/indirect effects of precipitation, P addition, and litter type with mass loss (Tian et al., 2021; Wade et al., 2026), based on a priori hypotheses (Fig. S2). Limited sample size prompted backward elimination ($|t| < 1.96$) to remove non-significant paths while retaining theoretical structure, yielding well-fitted final models.

3 Results

3.1 Litter mass loss and decomposition dynamics

Remaining litter mass declined significantly over the decomposition period. Overall, single-species litter decomposed faster than mixed-species litter, with total mass loss ranging from 31.07% to 57.06% (Table 1; Fig. 1). Precipitation and P additions significantly accelerated decomposition and reduced mean residence time (MRT), but their interaction was significant only in summer (Table S5; $p < 0.05$). The decomposition constant (k) of single-species litter increased with P concentration, whereas mixed-species litter showed no such response. Among single-species litter, the WHP treatment exhibited the fastest decomposition and shortest T_{95}, while mixed-species litter decomposition rates were highest under WMP and WHP treatments, with no significant difference between them (Table 1). RME analysis revealed a significant seasonal reversal in deviation from expected values for mixed-species litter decomposition: synergistic effects dominated in summer, whereas antagonistic effects prevailed in winter (Table S3; $p < 0.05$).

Litter nutrient remaining and chemical stoichiometry changed dynamically over time and differed seasonally (Table S5; Fig. 2). In summer, precipitation, P addition, and their interaction significantly accelerated the loss of C, N, lignin, and cellulose. P addition significantly promoted P loss, whereas precipitation had no significant effect (Fig. 2a, c; $p < 0.05$). Furthermore, precipitation addition, P addition, litter type, and their interactions all significantly affected chemical stoichiometry (Fig. 2b, d; $p < 0.05$). In winter, the pattern of precipitation-P interaction effects shifted markedly. Although precipitation and P addition continued to significantly accelerate C, N, and lignin loss ($p < 0.05$), their effects on P and cellulose loss were no longer significant (Fig. 2a, c; $p > 0.05$). Across all treatments, C, N, P, and cellulose loss decreased significantly, while remaining lignin remained relatively high, leading to continuously elevated lignin/N and lignin/P ratios. Notably, the interaction between precipitation and P addition significantly affected only the lignin/N ratio ($p < 0.05$). Moreover, litter type significantly influenced the loss of most nutrients and chemical stoichiometry in both seasons ($p < 0.05$). By the end of decomposition, single-species

litter generally exhibited greater C and cellulose loss and higher lignin remaining, coupled with higher C/P, N/P, and lignin/P ratios, but lower C/N and lignin/N ratios.

3.2 Dynamics of soil extracellular enzyme activities and CUE

The dynamic responses of soil physicochemical properties and microbial biomass to summer and winter precipitation and P addition are detailed in Appendix S8. The responses of soil extracellular enzyme activities to precipitation and P addition showed clear seasonal dynamics (Table S6; Fig. 3). In summer, precipitation addition significantly affected the activities of all enzyme indicators, while P addition only significantly affected the activities of BG, LAP, ALP, and POD. In winter, precipitation addition had significant effects on LAP, ALP, and the stoichiometric ratios of the five enzymes, while P addition only significantly affected BG, ALP, and PPO activities ($p < 0.05$). Additionally, the interaction between precipitation and litter type significantly affected the activities of PPO, ln(LAP)/ln(ALP), and ln(POD)/ln(LAP) in summer, and POD activity in winter ($p < 0.05$). BG activity was significantly promoted by the interaction of P addition and precipitation addition in both seasons. LAP activity was only significantly increased in summer, and precipitation addition alone significantly enhanced its activity in winter. ALP activity was significantly enhanced under ambient precipitation in summer and was generally inhibited in winter ($p < 0.05$). PPO activity was significantly enhanced only under precipitation addition in both seasons ($p < 0.05$), whereas POD activity was inhibited and only slightly increased under ambient precipitation in winter ($p > 0.05$). The stoichiometric ratios of enzymes further revealed the resource allocation strategies of microorganisms. P addition increased the ln(BG)/ln(LAP) ratio under ambient precipitation in single-species litter but decreased this ratio in mixed-species litter in summer. The ln(BG)/ln(ALP) ratio decreased in summer and increased under precipitation addition in winter ($p > 0.05$). The ln(POD)/ln(LAP) ratio in mixed-species litter was slightly promoted under ambient precipitation in winter ($p > 0.05$).

In summer, precipitation addition, P addition, litter type, and most of their interactions significantly affected CUE. The promoting effect of P addition on CUE disappeared in winter, and CUE was overall significantly lower in winter than in summer (Table S8; Fig. S4b, d; $p < 0.05$). In single-species litter, P addition promoted CUE in summer, and this positive effect was maintained only under precipitation addition in winter. In mixed-species litter, P addition showed a promoting effect in both seasons ($p < 0.05$). In contrast, NUE and PUE showed opposite trends to CUE.

3.3 Dynamics of microbial community structure and diversity

The flower plot shows that the number of bacterial s in winter was higher than that in summer, and the total number of core ASVs increased from approximately 95 to 170; the seasonal dynamics of fungal ASVs were different, with only 6 ASVs in summer and a narrower range in winter (Fig. S5). At the phylum level, summer bacterial communities were dominated by *Firmicutes*, and precipitation addition significantly increased the relative abundance of *Actinobacteria*; both precipitation and P addition significantly increased the abundance of *Proteobacteria* and *Bacteroidota* ($p < 0.05$). In winter, *Actinobacteria* and *Proteobacteria* became the dominant phyla, and the relative abundance of *Chloroflexota* and *Gemmatimonadota* also significantly increased, while the abundance of *Firmicutes* was significantly reduced by precipitation addition (Table S9; Fig. 4a; $p < 0.05$). In the fungal community, *Ascomycota* accounted for > 70% of the relative abundance year-round but declined in winter. P addition significantly altered *Ascomycota* abundance in winter, whereas *Basidiomycota* exhibited the opposite trend. At the genus level, *Brachymicrobium*, Bacillus, and *Arthrobacter* constituted the core group (Table S10; Fig. S6; $p < 0.05$). In summer, *Bacillus* and *Corynebacterium* were enriched in WHP and WMP treatments, and the relative abundance of *Arthrobacter*, *Devosia*, and *Paracoccus* increased in winter; in the fungal community, *Preussia* and *Cladosporium* maintained the core position throughout the year, while *Aspergillus* and other genera increased significantly in winter ($p < 0.05$).

Bacterial and fungal α-diversity exhibited opposite seasonal patterns, with mixed-species litter communities generally exhibiting lower α-diversity than single-species litter communities. Bacterial α-diversity was significantly lower in summer than in winter, whereas fungal α-diversity was significantly higher in summer than in winter (Table S11; Fig. 4b; $p < 0.05$). Precipitation and P additions significantly affected bacterial α-diversity in both summer and winter, and litter type became the dominant influencing factor in winter ($p < 0.05$). Fungal α-diversity displayed a P-dominated response pattern in summer, with precipitation addition significantly reducing most diversity indices. In winter, fungal α-diversity indices responded weakly to environmental factors, with only precipitation addition retaining a significant effect ($p < 0.05$). β-diversity analysis further revealed that bacterial communities exhibited significant differentiation along the precipitation gradient in summer, while inter-treatment differences diminished in winter. Fungal communities were sensitive to precipitation and P additions in summer; spatial overlap among samples increased in winter, and only P addition and litter type had significant effects (Table S12; Fig. 4c; $p < 0.05$).

3.4 Main drivers of litter decomposition

In summer, both types of litter mass loss were significantly positively correlated with LAP, BChao1, BObserved, BShannon, BAxis.1, and CUE, and significantly

negatively correlated with PPO, POD, BG/LAP, and POD/LAP (Fig. 5; $p < 0.05$). At the phylum level, *Proteobacteria* and *Bacteroidota* in both types of litter were significantly positively correlated with mass loss, BG, LAP, and CUE, and significantly negatively correlated with PPO, POD, and enzyme stoichiometric ratios ($p < 0.05$); *Firmicutes* showed the opposite pattern (Fig. S7; $p < 0.05$). At the genus level, *Devosia* was significantly positively correlated with mass loss, BG, LAP, and CUE (Fig. S8; $p < 0.05$); while *Corynebacterium* and *Planomicrobium* were significantly negatively correlated with mass loss, and significantly positively correlated with PPO, POD, and enzyme stoichiometric ratios ($p < 0.05$). In winter, the pattern of correlations changed significantly. In both types of litter, mass loss was significantly positively correlated with pH, BG/ALP, and NUE ($p < 0.05$). At the phylum level, *Actinobacteria* and *Basidiomycota* were significantly positively correlated with mass loss and PPO/POD, and at the genus level, *Planomicrobium* was significantly negatively correlated with mass loss ($p < 0.05$). In addition, bacterial and fungal communities were significantly correlated with most environmental indicators, and detailed results can be found in Appendix S9.

LEfSe and Simper analyses indicated that in summer, bacteria were dominated by *Firmicutes* (*Bacillus*), while in winter, *Proteobacteria* and *Actinobacteria* took the lead. The contribution of *Ornithinimicrobium* and *Balneimonas* in the mixed-species litter significantly increased (Fig. S9–S10). In summer, fungi were mainly *Ascomycota* (*Cladosporium*, *Alternaria*), while in winter, *Basidiomycota* (*Coprinellus*, *Schizophyllum*) and *Psychrophilic yeasts* (*Mrakia*, *Filobasidium*) dominated. Co-occurrence networks showed strong seasonal and litter-dependent statistical associations (Fig. 6a; Tables S13–S14). In summer, mixed-species litter networks had fewer nodes but higher connectivity; bacterial networks retained negative edges, while fungal networks were dominated by positive edges; in winter, bacterial network size expanded, although mixed-species litter remained lower than single-species litter. LMMs indicated that summer networks were regulated by the precipitation × P addition interaction and litter type, whereas winter networks were driven primarily by litter type ($p < 0.05$).

RDA analysis showed that environmental factors had a significant explanatory power for the variation in bacterial and fungal community structures (Fig. 6b; $p = 0.001$). In summer, water availability was the core driving factor for bacterial community differentiation; in winter, the communities tended to be homogenized, with bacteria mainly driven by enzyme activity and nutrient stoichiometric ratios, and fungi only responding significantly to P addition and litter type. Random forest models explained 39–62% of mass loss variance. %IncMSE highlighted soil available nutrients (AP, NH_4^+) and microbial stoichiometry (MBC/MBN) as key predictors across seasons (Fig. 6c), with AP and MBC/MBN dominating in summer and *Proteobacteria*/*Patescibacteria* in winter mixed-species litter models. PiecewiseSEM explained 73.6% (summer) and 63.0% (winter) of mass loss variance (Fig. 7). In summer, precipitation showed significant positive direct associations with both mass

loss and CUE (Fig. 7a; $p < 0.05$). Litter type had a significant positive direct association with mass loss. P addition exhibited a significant negative direct association with soil properties, but a positive direct association with the microbial community. CUE was significantly positively correlated with mass loss. In winter, precipitation showed significant positive direct associations with the microbial community, enzyme activity, CUE, and mass loss (Fig. 7b; $p < 0.05$). Litter type was negatively associated with the microbial community, but positively associated with mass loss. P addition had significant positive direct associations with both soil properties and the microbial community. Enzyme activity was negatively correlated with CUE in both seasons, and the direct effect of CUE on mass loss shifted to significantly negative in winter.

4 Discussion

4.1 P addition effects under hydrothermal thresholds and microbial physiological trade-offs

As expected, precipitation addition significantly accelerated decomposition of both litter types and shortened the time to reach 50% and 95% mass loss. However, its synergistic interaction with P addition was only evident during the summer window of high temperature and moisture (Tables 1–2; Fig. 1). This seasonal asymmetry supports the hypothesis of low temperature inhibition of decomposition (Parton et al., 2007). During the experimental period, summers were characterized by high temperatures and concentrated precipitation, forming a brief hydrothermal window; conversely, winters brought low temperatures and scarce rainfall, resulting in low temperature drought stress (Fig. S1). From the perspective of microbial resource economics, the underlying mechanism likely resides in the physiological trade-offs governing C allocation strategies in response to shifting hydrothermal regimes. In summer, P addition significantly promoted microbial biomass accumulation (MBC, MBN) and increased CUE. This indicates that P alleviated microbial P limitation, enabling greater C allocation to growth (Vitousek, 1994), consistent with Lian et al. (2025). SEM quantified this pathway: summer precipitation addition directly promoted mass loss and increased CUE, whereas P addition indirectly regulated decomposition by altering soil properties (increased AP, decreased SOC/TN) and community structure (*Proteobacteria* enrichment) (Fig. 7a).

Notably, decomposition did not cease entirely in winter, despite low temperatures. However, P addition suppressed MBC, and the positive response of CUE to P in single-species litter disappeared, remaining only under precipitation addition (Table S8; Fig. S4). The combination of low temperature and precipitation scarcity triggered a regulatory shift, forcing C allocation from growth to maintenance metabolism (Schimel et al., 2007; Lipson, 2015). SEM confirmed this transition, revealing that the effect of CUE on mass loss became negative in winter (Fig. 7b). This possibly reflects

a C shunting effect (Bolscher et al., 2024), whereby assimilated C is stored as intracellular polymers to sustain basal metabolism (Allison & Vitousek, 2005; Dijkstra et al., 2011). This physiological decoupling contrasts with the results of a recent global meta-analysis (Liu et al., 2024). The discrepancy may stem from limited energy metabolism in winter, which prevents microorganisms from utilizing available P sources even when present (Jia et al., 2026). Additionally, the slow decomposition of high-lignin components in mixed-species litter further amplified seasonal differences (Romero-Olivares et al., 2017). Therefore, simply extrapolating the globally observed promoting effect of P deposition to extreme arid regions may systematically overestimate winter C release. Future regional C cycle models must incorporate precipitation-temperature thresholds and seasonal CUE dynamics.

4.2 Seasonal reversal of non-additive mixing effects and the metabolic bottleneck

In this study, mixed-species litter decomposition did not exhibit the typical synergistic effect observed in traditional temperate ecosystems (Bai et al., 2026), but instead showed a significant seasonal reversal (Table S5). This supports the notion that the mixing effect is governed by chemical stoichiometric control of enzyme succession rather than physical contact (Gartner & Cardon, 2004; Hättenschwiler et al., 2005). In summer, mixed-species litter maintained higher CUE and decomposition rates by reducing BG/LAP, attributable to its wider initial C:N:P ratio and resource complementarity, demonstrating a synergistic effect (Sinsabaugh et al., 2009; Xiao et al., 2021). Increased water further amplified this effect (Li et al., 2026). However, this advantage disappeared in winter, reversing to an antagonistic effect. The initial lignin content of mixed-species litter was significantly higher than that of single-species litter (Table S1). Lignin-degrading PPO is highly temperature-sensitive, and low winter temperatures reduce substrate binding affinity and restrict de novo enzyme synthesis (Sinsabaugh et al., 2009; Xiao et al., 2021; Ma et al., 2023). Although winter precipitation addition significantly enriched Actinobacteria and promoted oxidative enzyme activities (PPO, POD/LAP), the downstream pathway linking enzyme activity to mass loss remained non-significant (Fig. 7b). This suggests that winter decomposition limitation stems from thermodynamic suppression of enzyme efficiency, rather than insufficient enzyme abundance or microbial functional diversity (Nannipieri et al., 2018; Tan et al., 2020; Alves et al., 2021). Consequently, single-species litter maintained baseline decomposition via labile C substrates, while mixed-species litter experienced severe metabolic bottlenecks under combined low temperature and physiological drought stress (Hättenschwiler et al., 2005; Zhou et al., 2020). SIMPER analysis indicated that seasonal community reorganization was the biological basis for this reversal (Fig. S10; Bao et al., 2025).

Based on these findings, we propose the "seasonal metabolic bottleneck hypothesis", wherein the non-additive effect of mixed-species litter shifts functionally as microbial strategies transition from "growth" to "survival". Significantly negative winter RME (WMP: −12.48%; WHP: −7.75%) and significant season-by-treatment interactions

strongly support this hypothesis (Tables S3–S4). Unlike the enzyme lock hypothesis, which emphasizes reversible inhibition of phenol oxidase by water, the metabolic bottleneck observed here stems from irreversible suppression of enzyme catalytic efficiency by low temperatures, amplified by substrate chemical stoichiometry (Schimel et al., 2007). Additionally, altered litterbag ventilation or phenolic allelochemical accumulation may act synergistically (Orwin et al., 2011). However, winter precipitation addition boosted community and oxidative enzyme activity yet failed to overcome the mass loss bottleneck, supporting thermodynamic limitation of lignin degradation as the primary cause (Tan et al., 2020; Alves et al., 2021). Notably, even under ambient winter precipitation, mixed-species litter modulated oxidative-to-hydrolytic enzyme ratios and maintained positive nutrient use efficiency correlations (Fig. 3b, 5), indicating that resource complementarity buffering is strictly dependent on hydrothermal activation thresholds (Joly et al., 2017; Li et al., 2024). These findings refute the traditional view of stable litter mixing effects across environments, indicating that strong environmental filtering in extreme arid regions masks resource complementarity and drives seasonal functional reversal (Zhou et al., 2020; Bai et al., 2026). Although intense arid ultraviolet radiation breaks down recalcitrant litter structures, subsequent microbial mineralization remains hydrothermally constrained, further explaining the seasonal disappearance of complementarity effects (Gallo et al., 2009; Liu et al., 2025).

4.3 Microbial community assembly, shifts in enzymatic investment strategies, and cascading regulatory mechanisms

Microbial community succession was highly coupled with shifts in enzyme investment strategies, driving seasonal dynamics of decomposition (Sinsabaugh et al., 2009; Manzoni et al., 2012). In summer, hydrothermal suitability favored fast-growing opportunistic microbial taxa, with dominant bacterial phyla *Firmicutes* (e.g., *Bacillus*) and fungal phylum *Ascomycota* (e.g., *Cladosporium*, *Alternaria*) rapidly proliferating under favorable conditions (Fig. S5, S8–S9; Voříšková & Baldrian, 2013). However, SEM and correlation analyses identified *Proteobacteria* and bacterial Shannon diversity as the core functional hubs driving decomposition and CUE increases. These were positively correlated with BG and LAP, consistent with a high-CUE "get-then-grow" strategy (Fig. 5, 7a; Fig. S7–S8). Conversely, abundant Bacillus were likely dormant and did not drive CUE increases, indicating that quantitative dominance does not equal functional contribution in extreme arid ecosystems (Blagodatskaya & Kuzyakov, 2013; Hansen et al., 2026). Notably, lower bacterial α-diversity in summer versus winter did not indicate functional degradation (Fig. 4b). Although summer *Firmicutes* outbreaks reduced evenness, rising Shannon diversity across treatments remained a key CUE mediator. In winter, despite higher bacterial α-diversity, functions were dominated by stress-tolerant or limited key taxa, and Shannon was not significantly linked to CUE pathways (Fig. 7b). This decoupling of abundance/diversity from functional contribution highlights the disconnect between

590 microbial community structure and ecological function in extreme arid regions
591 (Blagodatskaya & Kuzyakov, 2013; Schnecker et al., 2023).
592
593 In winter, communities shifted to stress-tolerant taxa, including *Actinobacteria*,
594 *Basidiomycota* (e.g., *Coprinellus*, *Schizophyllum*), and *Psychrophilic yeasts* (e.g.,
595 *Mrakia*, *Filobasidium*). SEM revealed that *Actinobacteria* directly increased PPO
596 activity, driving a recalcitrant C mining strategy. POD correlated positively with
597 *Basidiomycota*, indicating fungal peroxidase participation in recalcitrant C oxidation
598 (Gong et al., 2023). Extreme cold suppressed metabolic activity, forcing survival
599 strategies with low CUE and high oxidase activity (Thomas-Hall et al., 2010;
600 Manzoni et al., 2012; Sun et al., 2024). Mixed-species litter buffered this via
601 functional redundancy from specific taxa (e.g., *Ornithinimicrobium*, *Balneimonas*)
602 (Zhou et al., 2020). Co-occurrence network analysis suggests this buffering effect
603 stems from reorganized taxon association patterns (Bao et al., 2025). Higher
604 proportions of negative edges in bacterial networks may reflect resource competition
605 and niche differentiation (Yang et al., 2024b), whereas positive-edge dominance in
606 fungal networks implies synergistic stress responses (Xiao & Chen, 2021). LMMs
607 identified winter litter type as the dominant driver of network complexity (Table S14).
608 This substrate-quality-driven reorganization failed to overcome thermodynamic limits,
609 corroborating the seasonal metabolic bottleneck hypothesis at the community level.
610 RDA indicated water availability drove summer bacterial differentiation; in winter,
611 environmental factors explained less variation, and communities homogenized (Fig.
612 6b). As decomposition progressed, single-species litter assembly was primarily abiotic
613 (AP, inorganic N). In mixed-species litter, winter core predictors shifted from
614 physicochemical factors to community structure (e.g., *Proteobacteria*,
615 *Patescibacteria*), with increased fungal spatial overlap (Table S12; Fig. 4c),
616 weakening fungal assembly responses to hydrothermal conditions (Lian et al., 2025).
617 This shift from abiotic selection to joint biotic-substrate drivers further confirms
618 microbial community assembly strategies crossing hydrothermal thresholds.
619
620 The seasonal transition in community assembly and enzyme investment strategies
621 manifested as cascading microbial C allocation trade-offs. Seasonal trade-offs among
622 CUE, NUE, and PUE reflected fundamental microbial resource allocation economics
623 (Sinsabaugh et al., 2013; Lipson, 2015). SEM further supported this cascading
624 regulation, indicating that the community-level switch from "growth" to "survival"
625 strategies led to decreased CUE and increased enzyme investment, diverting
626 enzymatic products toward assimilatory storage rather than respiratory release,
627 functionally supporting a "conservative survival strategy" in winter (Bolscher et al.,
628 2024). This implies that simply setting winter decomposition rates to "zero" or a
629 constant would underestimate C turnover during the non-growing season in arid
630 regions.
631
632 4.4 Implications of the winter metabolic bottleneck for C-cycle models and study

limitations

Long cold seasons and physiological drought maintain arid microbial communities in low-activity states, producing pulsed litter C release (Schimel et al., 2007; Imminger et al., 2024). Despite low-temperature suppression, winter litter mass loss showed microbial metabolism persisted (Fig. 1–2), challenging steady-state assumptions of traditional models treating winter decomposition as zero or constant (Olson, 1963). Our 720-day observation confirmed that incorporating the cascade "hydrothermal thresholds → microbial trade-offs → community assembly and enzyme stoichiometry" accurately depicts decomposition dynamics in extreme arid regions. Future arid C cycle models should incorporate seasonal CUE reversal, temperature-sensitive oxidase-hydrolase stoichiometry, and microbial network topology. Limitations include: (1) 1-mm mesh excluding macrofauna, potentially underestimating fragmentation; (2) undifferentiated bioavailability among mineral P forms; (3) lack of quantitative lignin data (e.g., FTIR/NMR), limiting photodegradation-microbial coupling analysis; (4) indirect CUE estimation via eco-enzymatic stoichiometry, with negative winter values reflecting model outputs rather than direct measurements under non-steady-state conditions; (5) need for multi-site validation of the seasonal metabolic bottleneck hypothesis; (6) unquantified UV-B blocking and photodegradation priming effects on microbial colonization. Future work should address these gaps using substrate-induced respiration or stable isotope labeling.

5 Conclusion

In summer, precipitation and P addition synergistically alleviate P limitation, enhancing CUE and directing C to growth metabolism. In winter, low temperatures and physiological drought block this pathway, redirecting assimilated C to intracellular storage for basal metabolism. This growth-to-survival C allocation trade-off underpins seasonal decomposition asynchrony. Mixed-species non-additive effects also depend on this threshold: summer synergy arises from substrate stoichiometric complementarity and hydrolase-driven high CUE, whereas winter antagonism results from lignin-impeded oxidative degradation and a metabolic bottleneck overriding functional complementarity. The core mechanism involves synchronous shifts in community structure and enzyme strategies—summer decomposition and CUE are driven by *Proteobacteria* and bacterial Shannon diversity, while winter recalcitrant C mining relies on *Actinobacteria*-mediated PPO activity. Despite massive winter enzyme synthesis, decomposition remains limited by thermodynamic suppression of catalytic efficiency rather than enzyme quantity. Substrate-driven network reorganization fails to overcome this, corroborating the seasonal metabolic bottleneck hypothesis. These findings indicate decomposition is driven not by linear annual climate effects but by dynamic substrate–microbial adaptation across thresholds; ignoring this misjudges non-growing season C turnover in models.

Acknowledgments

This work was funded by the Tianshan Yingcai Program of Xinjiang Uygur Autonomous Region (2024TSYCLJ0028), the National Natural Science Foundation of China (42171066) and the third Xinjiang Scientific Expedition Program (2022xjkk1503).

Declaration of competing interest

The authors declare that they have no known competing financial interests or personal relationships that could have appeared to influence the work reported in this paper.

Data availability

Processed data are provided in the https://www.kdocs.cn/l/cdlBivvhU7re.

References

Allison SD, Vitousek PM (2005) Responses of extracellular enzymes to simple and complex nutrient inputs. Soil Biol Biochem 37:937–944. https://doi.org/10.1016/j.soilbio.2004.09.014

Alves RJE, Callejas IA, Marschmann GL, Mooshammer M, Singh HW, Whitney B, et al (2021) Kinetic properties of microbial exoenzymes vary with soil depth but have similar temperature sensitivities through the soil profile. Front Microbiol 12:735282. https://doi.org/10.3389/fmicb.2021.735282

Austin AT, Ballaré CL (2024) Photodegradation in terrestrial ecosystems. New Phytol 244:769–785. https://doi.org/10.1111/nph.20105

Bai L, Song C, Li M, Yang L, Wang X, Wu Q, et al (2026) Global patterns and drivers of decomposition of mixed-species litter. Geoderma 465:117662. https://doi.org/10.1016/j.geoderma.2025.117662

Bao R, Tang K, Ji Y, Zhang S, Wang C, Liang Y, Zhao X, Meng J (2025) Spatiotemporal dynamics of bacterial community assembly and co-occurrence patterns in biological soil crusts of desert ecosystems. Microorganisms 13:446. https://doi.org/10.3390/microorganisms13020446

Berglund SL, Ågren GI (2012) When will litter mixtures decompose faster or slower than individual litters? A model for two litters. Oikos 121:1112–1120. https://doi.org/10.1111/j.1600-0706.2011.19787.x

Bolscher T, Vogel C, Olagoke FK, Meurer KHE, Herrmann AM, Colombi T, et al (2024) Beyond growth: the significance of non-growth anabolism for microbial C-use efficiency in the light of soil C stabilisation. Soil Biol Biochem 193:109400. https://doi.org/10.1016/j.soilbio.2024.109400

Brookes PC, Landman A, Pruden G, Jenkinson DS (1985) Chloroform fumigation and the release of soil nitrogen: a rapid direct extraction method to measure microbial biomass nitrogen in soil. Soil Biol Biochem 17:837–842. https://doi.org/10.1016/0038-0717(85)90144-0

Callahan BJ, McMurdie PJ, Rosen MJ, Han AW, Johnson AJA, Holmes SP (2016) DADA2: High-resolution sample inference from Illumina amplicon data. Nat Methods 13:581–583. https://doi.org/10.1038/nmeth.3869
Chen C, Xiao W (2023) The global positive effect of phosphorus addition on soil microbial biomass. Soil Biol Biochem 176:108882. https://doi.org/10.1016/j.soilbio.2022.108882
Cui Y, Hu J, Peng S, Delgado-Baquerizo M, Moorhead DL, Sinsabaugh RL, et al (2024) Limiting resources define the global pattern of soil microbial carbon use efficiency. Adv Sci 11:2308176. https://doi.org/10.1002/advs.202308176
Day TA, Urbine JM, Bliss MS (2022) Supplemental precipitation accelerates decay but only in photodegraded litter and implications that sunlight promotes leaching loss. Biogeochemistry 158:113–129. https://doi.org/10.1007/s10533-022-00888-x
DeForest JL (2009) The influence of time, storage temperature, and substrate age on potential soil enzyme activity in acidic forest soils using MUB-linked substrates and L-DOPA. Soil Biol Biochem 41:1180–1186. https://doi.org/10.1016/j.soilbio.2009.02.029
Dijkstra P, Thomas SC, Heinrich PL, Koch GW, Schwartz E (2011) Effect of temperature on metabolic activity of intact microbial communities: evidence for altered metabolic pathway activity but not for increased maintenance respiration and reduced C use efficiency. Soil Biol Biochem 43:2023–2031. https://doi.org/10.1016/j.soilbio.2011.05.018
Fan LJ, Li CD, Li XY, Sun HJ, Lin LS, Liu B (2021) Effects of sand burial on litter decomposition rate and salt content dynamics in an extremely arid region. Chin J Plant Ecol 45:144–153. https://doi.org/10.17521/cjpe.2020.0273
Gallo ME, Porras-Alfaro A, Odenbach KJ, Sinsabaugh RL (2009) Photoacceleration of plant litter decomposition in an arid environment. Soil Biol Biochem 41:1433–1441. https://doi.org/10.1016/j.soilbio.2009.03.025
Gao Y, Tariq A, Zeng FJ, Sardans J, Al-Bakre DA, Peñuelas J (2024) Fractions of soil P mediated by rhizospheric phoD-harbouring bacteria of deep-rooted desert species are determined by fine-root traits. Funct Ecol 38:2300–2315. https://doi.org/10.1111/1365-2435.14635
Gao Y, Tariq A, Zeng FJ, Li XY, Sardans J, Al-Bakre DA, et al (2025) Metagenomics reveals divergent functional profiles of soil C and nitrogen cycles in an experimental drought and P-poor desert ecosystem. Appl Soil Ecol 207:105946. https://doi.org/10.1016/j.apsoil.2025.105946
Gartner TB, Cardon ZG (2004) Leaf litter mixtures and their effects on decomposition: a meta-analysis. Ecology 85:2077–2086. https://doi.org/10.1890/03-0662
Gong JR, Zhang ZH, Zhu CC, Shi JY, Zhang WY, Song LY, et al (2022) The response of litter decomposition to P addition in typical temperate grassland in Inner Mongolia. J Arid Environ 197:104677. https://doi.org/10.1016/j.jaridenv.2021.104677
Gong JR, Dong XD, Li XB, Yue KX, Shi JY, Song LY, et al (2023) P fertilization affects litter quality and enzyme activity in a semiarid grassland. Plant Soil 492:91–108. https://doi.org/10.1007/s11104-023-06153-w
Hansen PM, Zhang Y, Guseva K, Kaiser C, Cotrufo MF (2026) Microbial community

759 regulation of extracellular enzyme production can mediate patterns of particulate and
760 mineral-associated organic matter accumulation in undersaturated soils. Soil Biol
761 Biochem 214:110056. https://doi.org/10.1016/j.soilbio.2025.110056
762 Hättenschwiler S, Tiunov AV, Scheu S (2005) Biodiversity and litter decomposition in
763 terrestrial ecosystems. Annu Rev Ecol Evol Syst 36:191–218.
764 https://doi.org/10.1146/annurev.ecolsys.36.091704.085500
765 Hou SL, Hättenschwiler S, Yang JJ, Sistla S, Wei HW, Zhang ZW, et al (2021)
766 Increasing rates of long-term nitrogen deposition consistently increased litter
767 decomposition in a semi-arid grassland. New Phytol 229:296–307.
768 https://doi.org/10.1111/nph.16854
769 Imminger S, Meier DV, Schintlmeister A, Legin A, Schnecker J, Richter A, et al (2024)
770 Survival and rapid resuscitation permit limited productivity in desert microbial
771 communities. Nat Commun 15:3056. https://doi.org/10.1038/s41467-024-46920-6
772 Jameson BD, Murdock SA, Ji Q, Stevens CJ, Grundle DS, Juniper SK (2023)
773 Network analysis of 16S rRNA sequences suggests microbial keystone taxa contribute
774 to marine N2O cycling. Commun Biol 6:212.
775 https://doi.org/10.1038/s42003-023-04597-5
776 Jefferies RL, Walker NA, Edwards KA, Lundberg P, Sullivan PF (2010) Is the decline
777 of soil microbial biomass in late winter coupled to changes in the physical state of
778 cold soils? Soil Biol Biochem 42:129–135.
779 https://doi.org/10.1016/j.soilbio.2009.10.008
780 Jenkinson DS, Powlson DS (1976) The effects of biocidal treatments on metabolism
781 in soil—I. Fumigation with chloroform. Soil Biol Biochem 8:167–177.
782 https://doi.org/10.1016/0038-0717(76)80001-8
783 Jia Z, Wu P, Liu X, Wang H, Zhu F, Qin S (2026) Temperature regulates the effects of
784 N and P addition on straw decomposition and soil organic C dynamic in black soil.
785 Soil Ecol Lett 8:260433. https://doi.org/10.1007/s42832-026-0433-4
786 Joly FX, Kurupas KL, Throop HL (2017) Pulse frequency and soil-litter mixing alter
787 the control of cumulative precipitation over litter decomposition. Ecology 98:2255–
788 2260. https://doi.org/10.1002/ecy.1931
789 Li ZL, Peng Q, Dong YS, Guo Y (2022) The influence of increased precipitation and
790 nitrogen deposition on the litter decomposition and soil microbial community
791 structure in a semiarid grassland. Sci Total Environ 844:157115.
792 https://doi.org/10.1016/j.scitotenv.2022.157115
793 Li JW, Wu JZ, Yu JY, Wang KB, Li JP, Cui YX, et al (2024) Soil enzyme activity and
794 stoichiometry in response to precipitation changes in terrestrial ecosystems. Soil Biol
795 Biochem 191:109321. https://doi.org/10.1016/j.soilbio.2024.109321
796 Li M, Liu Y, Wang P, Li X (2026) Precipitation and P addition jointly regulate litter
797 decomposition by altering litter stoichiometry and extracellular enzyme activity. J
798 Arid Environ 237:105720. https://doi.org/10.1016/j.jaridenv.2026.105720
799 Lian J, Chen J, Han C, Zhao Y, Yang X, Li J (2025) Soil extracellular enzyme
800 stoichiometry reveals the nutrient limitations of soil microbial metabolism under
801 precipitation changes in Ningxia desert steppe of China. Eur J Soil Biol 127:103774.
802 https://doi.org/10.1016/j.ejsobi.2025.103774

Lipson DA (2015) The complex relationship between microbial growth rate and yield and its implications for ecosystem processes. Front Microbiol 6:615. https://doi.org/10.3389/fmicb.2015.00615
Liu YL, Zhang AL, Li XY, Kuang WN, Islam W (2024) Litter decomposition rate response to multiple global change factors: a meta-analysis. Soil Biol Biochem 197:109533. https://doi.org/10.1016/j.soilbio.2024.109533
Liu YL, Li L, Zhang ZH, Li XY, Zhang AL, Wang SQ (2025) Ultraviolet radiation effects on biodegradation depend on precipitation amount, litter quality, and time in an arid land. Appl Soil Ecol 215:106451. https://doi.org/10.1016/j.apsoil.2025.106451
Ma Z, Chen Y, Xu W, Liu M (2023) Effects of warming on the stoichiometry of soil microbial biomass and extracellular enzymes in an alpine shrubland. Geoderma 430:116329. https://doi.org/10.1016/j.geoderma.2023.116329
Manzoni S, Taylor P, Richter A, Porporato AMM, Ågren GI (2012) Environmental and stoichiometric controls on microbial C-use efficiency in soils. New Phytol 196:79–91. https://doi.org/10.1111/j.1469-8137.2012.04225.x
Nannipieri P, Trasar-Cepeda C, Dick RP (2018) Soil enzyme activity: a brief history and biochemistry as a basis for appropriate interpretations and meta-analysis. Biol Fertil Soils 54:11–19. https://doi.org/10.1007/s00374-017-1245-6
Nilsson RH, Larsson K-H, Taylor AFS, Bengtsson-Palme J, Jeppesen TS, Schigel D, Kennedy P, Picard K, Glöckner FO, Tedersoo L, Saar I, Kõljalg U, Abarenkov K (2019) The UNITE database for molecular identification of fungi: handling dark taxa and parallel taxonomic classifications. Nucleic Acids Res 47:D259–D264. https://doi.org/10.1093/nar/gky1022
Olson JS (1963) Energy storage and the balance of producers and decomposers in ecological systems. Ecology 44:322–331. https://doi.org/10.2307/1932179
Orwin KH, Wardle DA, Greenfield LG (2011) Do tannins and other plant secondary metabolites constrain decomposition in lowland rain forests? A laboratory experiment. Oecologia 167:1053–1063. https://doi.org/10.1007/s00442-011-2063-2
Pan Y, Liu B, Cao J, Liu J, Tian S, Du E (2021) Enhanced atmospheric P deposition in Asia and Europe in the past two decades. Atmos Ocean Sci Lett 14:100051. https://doi.org/10.1016/j.aosl.2021.100051
Parton WJ, Silver WL, Burke IC, Grassens L, Harmon ME, Currie WS, et al (2007) Global-scale similarities in nitrogen release patterns during long-term decomposition. Science 315:361–364. https://doi.org/10.1126/science.1134853
Qu H, Medina-Roldán E, Wang S, Ma X, Wang X, Tang X, et al (2024) A 5-and-a-half-year-experiment shows precipitation thresholds in litter decomposition and nutrient dynamics in arid and semi-arid regions. Biol Fertil Soils 60:199–212. https://doi.org/10.1007/s00374-023-01779-5
Quast C, Pruesse E, Yilmaz P, Gerken J, Schweer T, Yarza P, Peplies J, Glöckner FO (2013) The SILVA ribosomal RNA gene database project: improved data processing and web-based tools. Nucleic Acids Res 41:D590–D596. https://doi.org/10.1093/nar/gks1219
Romero-Olivares AL, Allison SD, Treseder KK (2017) Decomposition of recalcitrant C under experimental warming in boreal forest. PLoS ONE 12:e0179674.

https://doi.org/10.1371/journal.pone.0179674
Saiya-Cork KR, Sinsabaugh RL, Zak DR (2002) The effects of long-term nitrogen deposition on extracellular enzyme activity in an Acer saccharum forest soil. Soil Biol Biochem 34:1309–1315. https://doi.org/10.1016/S0038-0717(02)00074-3
Schimel JP, Balser TC, Wallenstein M (2007) Microbial stress-response physiology and the structure and function of soil microbial communities. Soil Sci Soc Am J 71:1123–1133. https://doi.org/10.2136/sssaj2006.0309
Schnecker J, Baldaszti L, Gündler P, Pleitner M, Sandén T, Simon E, et al (2023) Seasonal dynamics of soil microbial growth, respiration, biomass, and C use efficiency in temperate soils. Geoderma 440:116693. https://doi.org/10.1016/j.geoderma.2023.116693
Shi JY, Gong JR, Baoyin TT, Luo QP, Zhai ZW, Zhang ZH, et al (2021) Short-term P addition increases soil respiration by promoting gross ecosystem production and litter decomposition in a typical temperate grassland in northern China. Catena 197:104952. https://doi.org/10.1016/j.catena.2020.104952
Sinsabaugh RL, Hill BH, Shah JJF (2009) Ecoenzymatic stoichiometry of microbial organic nutrient acquisition in soil and sediment. Nature 462:795–798. https://doi.org/10.1038/nature08632
Sinsabaugh RL, Manzoni S, Moorhead DL, Richter A (2013) C use efficiency of microbial communities: stoichiometry, methodology and modelling. Ecol Lett 16:930–939. https://doi.org/10.1111/ele.12113
Sun L, Qu L, Moorhead DL, Cui Y, Wanek W, Li S, et al (2024) Interpreting the differences in microbial carbon and nitrogen use efficiencies estimated by 18O labeling and ecoenzyme stoichiometry. Geoderma 444:116856. https://doi.org/10.1016/j.geoderma.2024.116856
Tan X, Machmuller MB, Huang F, He J, Chen J, Cotrufo MF, et al (2020) Temperature sensitivity of ecoenzyme kinetics driving litter decomposition. Soil Biol Biochem 148:107878. https://doi.org/10.1016/j.soilbio.2020.107878
Thomas-Hall SR, Turchetti B, Buzzini P, Branda E, Boekhout T, Theelen B, Watson K (2010) Cold-adapted yeasts from Antarctica and the Italian Alps—description of three novel species: Mrakia robertii sp. nov., Mrakia blollopis sp. nov. and Mrakiella niccombsii sp. nov. Extremophiles 14:47–59. https://doi.org/10.1007/s00792-009-0286-7
Tian P, Liu S, Zhao X, Sun ZL, Yao X, Niu SL, et al (2021) Past climate conditions predict the influence of nitrogen enrichment on the temperature sensitivity of soil respiration. Commun Earth Environ 2:251. https://doi.org/10.1038/s43247-021-00324-2
Tipping E, Benham S, Boyle JF, Crow P, Davies J, Fischer U, et al (2014) Atmospheric deposition of phosphorus to land and freshwater. Environ Sci Process Impacts 16:1608. https://doi.org/10.1039/C3EM00641G
Van Soest PJ (1967) Development of a comprehensive system of feed analyses and its application to forages. J Anim Sci 26:119–128. https://doi.org/10.2527/jas1967.261119x
Vance ED, Brookes PC, Jenkinson DS (1987) An extraction method for measuring

soil microbial biomass C. Soil Biol Biochem 19:703–706. https://doi.org/10.1016/0038-0717(87)90052-6
Vitousek PM (1994) Nutrient cycling and nutrient limitation in tropical forest ecosystems. Princeton University Press, Princeton
Voříšková J, Baldrian P (2013) Fungal community on decomposing leaf litter undergoes rapid successional changes. FEMS Microbiol Ecol 85:273–285. https://doi.org/10.1111/1574-6941.12120
Wade J, Potter TM, Margenot AJ (2026) Commentary: Structural equation models and causal claims in soil science and biogeochemistry – An equation-free "how to". Geoderma 466:117702. https://doi.org/10.1016/j.geoderma.2026.117702
Wahdan SFM, Ji L, Schädler M, Wu YT, Sansupa C, Tanunchai B, et al (2023) Future climate conditions accelerate wheat straw decomposition alongside altered microbial community composition, assembly patterns, and co-occurrence networks. ISME J 17:238–251. https://doi.org/10.1038/s41396-022-01336-2
Wang QW, Pieristè M, Liu C, Kenta T, Robson TM, Kurokawa H, et al (2020) The contribution of photodegradation to litter decomposition in a temperate forest gap and understorey. New Phytol 229:2625–2636. https://doi.org/10.1111/nph.17011
Xiao W, Chen C, Chen X, Huang Z, Chen HYH (2021) Functional and phylogenetic diversity promote litter decomposition across terrestrial ecosystems. Ecol Lett 23:1488–1499. https://doi.org/10.1111/ele.13561
Yang L, Canarini A, Zhang W, Lang M, Chen Y, Cui Z, et al (2024a) Microbial life-history strategies mediate microbial C pump efficacy in response to N management depending on stoichiometry of microbial demand. Glob Change Biol 30:e17311. https://doi.org/10.1111/gcb.17311
Yang X, Jiang N, Sun D (2024b) Dry-wet cycles induce the decoupling of C and nitrogen mineralization at high temperatures in semi-arid grassland soil. Soil Biol Biochem 188:109227. https://doi.org/10.1016/j.soilbio.2023.109227
Zheng H, Yang T, Bao Y, He P, Yang K, Mei X, et al (2021) Network analysis and subsequent culturing reveal keystone taxa involved in microbial litter decomposition dynamics. Soil Biol Biochem 157:108230. https://doi.org/10.1016/j.soilbio.2021.108230
Zhou SX, Butenschoen O, Barantal S, Handa IT, Makkonen M, Vos V, et al (2020) Decomposition of leaf litter mixtures across biomes: the role of litter identity, diversity and soil fauna. J Ecol 108:2374–2385. https://doi.org/10.1111/1365-2745.13452
Zhou SX, Butenschoen O, Barantal S, Handa IT, McKie B, Huang C, et al (2024) Litter mixture effects on nitrogen dynamics during decomposition predominantly vary among biomes but little with litter identity, diversity and soil fauna. Soil Biol Biochem 199:109602. https://doi.org/10.1016/j.soilbio.2024.109602

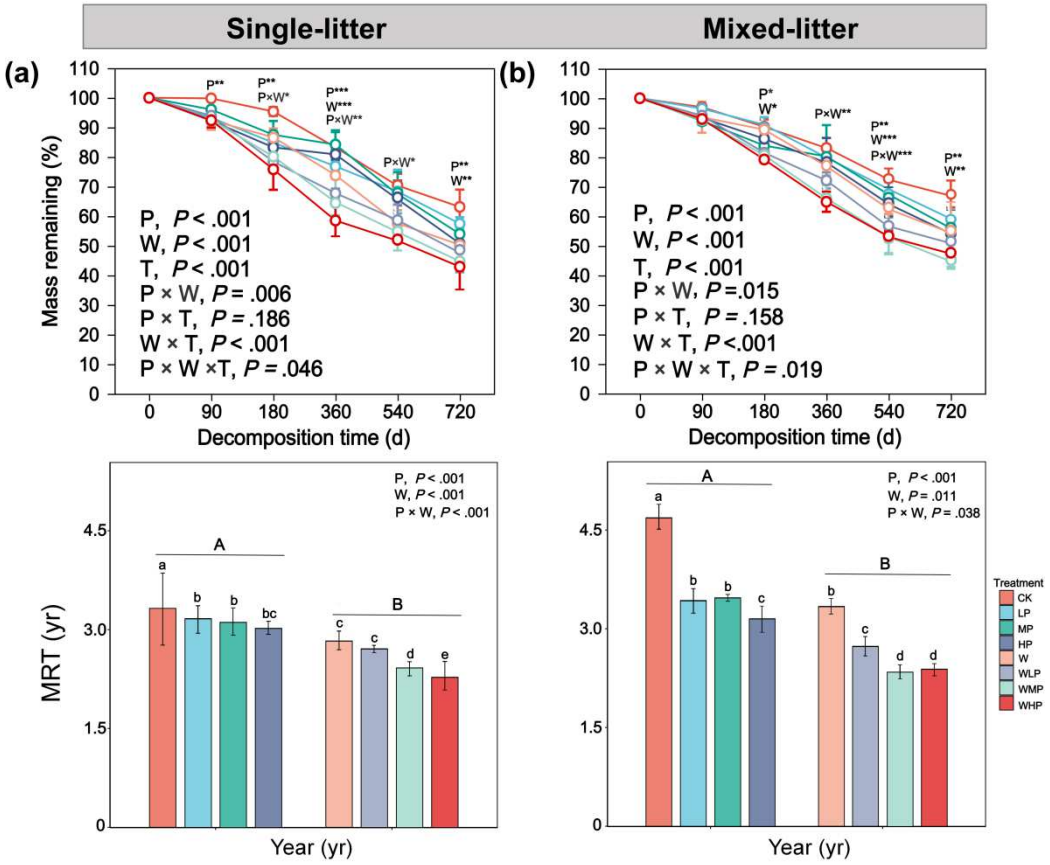


Fig. 1 Dynamics of mass remaining and mean residence time for single-species (**a**) and mixed-species (**b**) litter. P: P addition effect; W: precipitation addition effect; T: decomposition time; P × W: interactive effect of P and precipitation addition; P × T: interactive effect of P addition and time; W × T: interactive effect of precipitation addition and time; P × W × T: three-way interaction among P, W, and T. CK: ambient precipitation + P deposition; W: with 50% of maximum ambient precipitation addition; LP: with 1 g P m^{-2} yr^{-1} P addition; MP: with 2.5 g P m^{-2} yr^{-1} P addition; HP: with 5 g P m^{-2} yr^{-1} P addition; WLP: with both W + LP treatments; WMP: with both W + MP treatments; WHP: with both W + HP treatments. Different lowercase letters indicate significant differences among treatments. Error bars represent standard errors of the means ($n = 3$, ***$p < 0.001$, **$p < 0.01$, and *$p < 0.05$).

942 Table 1 Decomposition rate constant (k) and model-estimated time to reach 50% ($T_{50\%}$) and 95% ($T_{95\%}$) mass loss.

Species	Treatments	k (g^{-1} a^{-1})	R^2	p	$T_{50\%}$	$T_{95\%}$
Single-litter	CK	0.272±0.003e	0.966	< 0.001	2.55	11.02
	LP	0.284±0.023d	0.955	< 0.001	2.44	10.54
	MP	0.295±0.004d	0.912	< 0.001	2.35	10.16
	HP	0.326±0.011cd	0.917	< 0.001	2.12	9.18
	W	0.346±0.014c	0.936	< 0.001	2.01	9.67
	WLP	0.379±0.004c	0.963	< 0.001	1.83	7.91
	WMP	0.426±0.006b	0.974	< 0.001	1.63	7.03
	WHP	0.436±0.011a	0.920	< 0.001	1.60	6.29
Mixed-litter	CK	0.201±0.008d	0.989	< 0.001	3.45	14.90
	LP	0.283±0.019c	0.988	< 0.001	2.45	10.60
	MP	0.280±0.008c	0.963	< 0.001	2.48	10.70
	HP	0.314±0.016b	0.917	< 0.001	2.21	9.56
	W	0.276±0.004c	0.951	< 0.001	2.52	10.87
	WLP	0.362±0.013b	0.978	< 0.001	1.91	8.28
	WMP	0.418±0.021a	0.981	< 0.001	1.66	7.17
	WHP	0.404±0.009a	0.960	< 0.001	1.72	7.41

944 Note: different lowercase letters within a column denote significant differences
945 among treatments. Values are means ± SE (n = 3, p < 0.05). Treatment descriptions
946 are provided in Fig. 1.
947

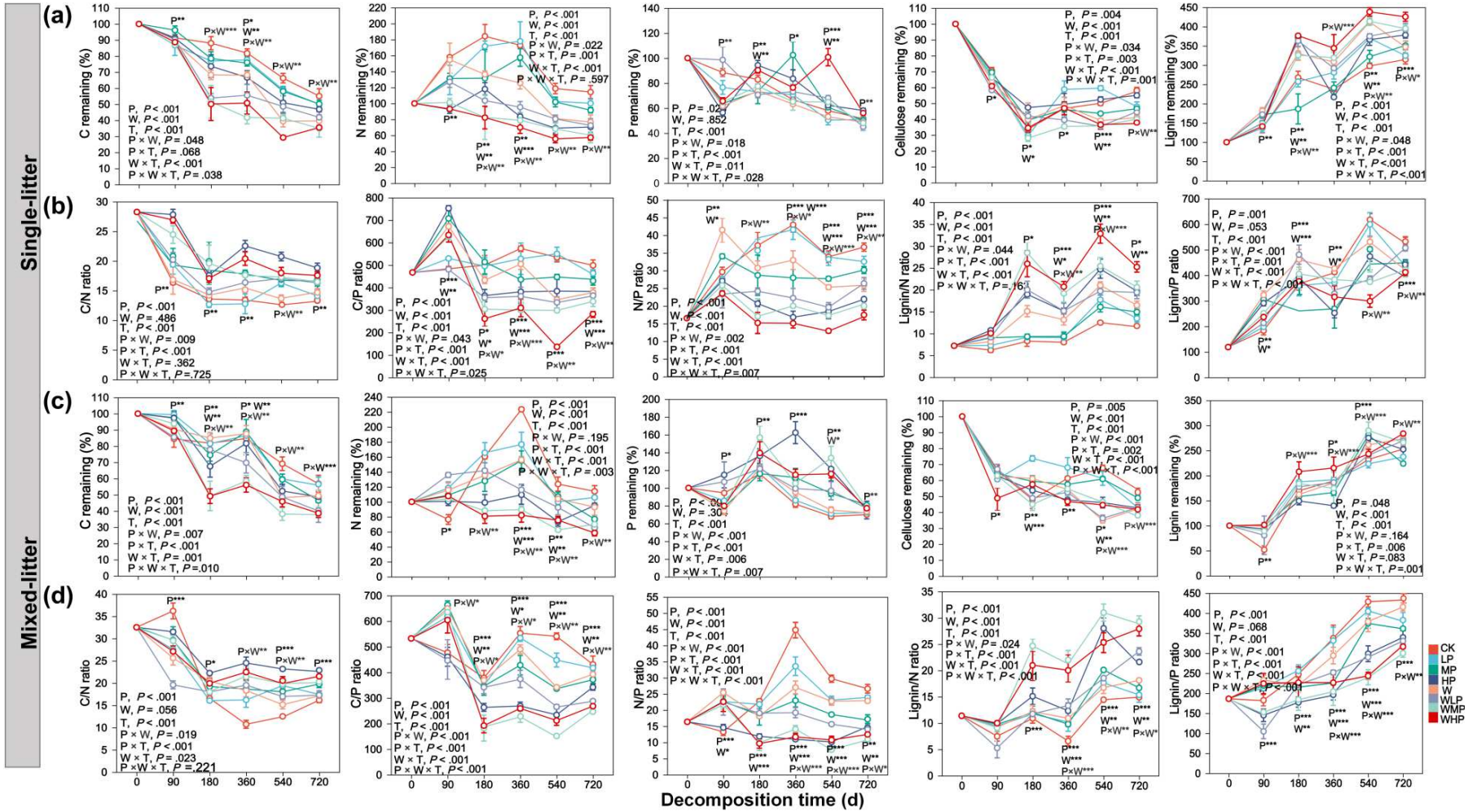


Fig. 2 Dynamics of nutrient remaining and stoichiometric ratios of single-species (**a, b**) and mixed-species (**c, d**) litter. Error bars represent standard errors of the means ($n = 3$, $^{***}p < 0.001$, $^{**}p < 0.01$, and $^{*}p < 0.05$). Treatment descriptions are provided in Fig. 1.

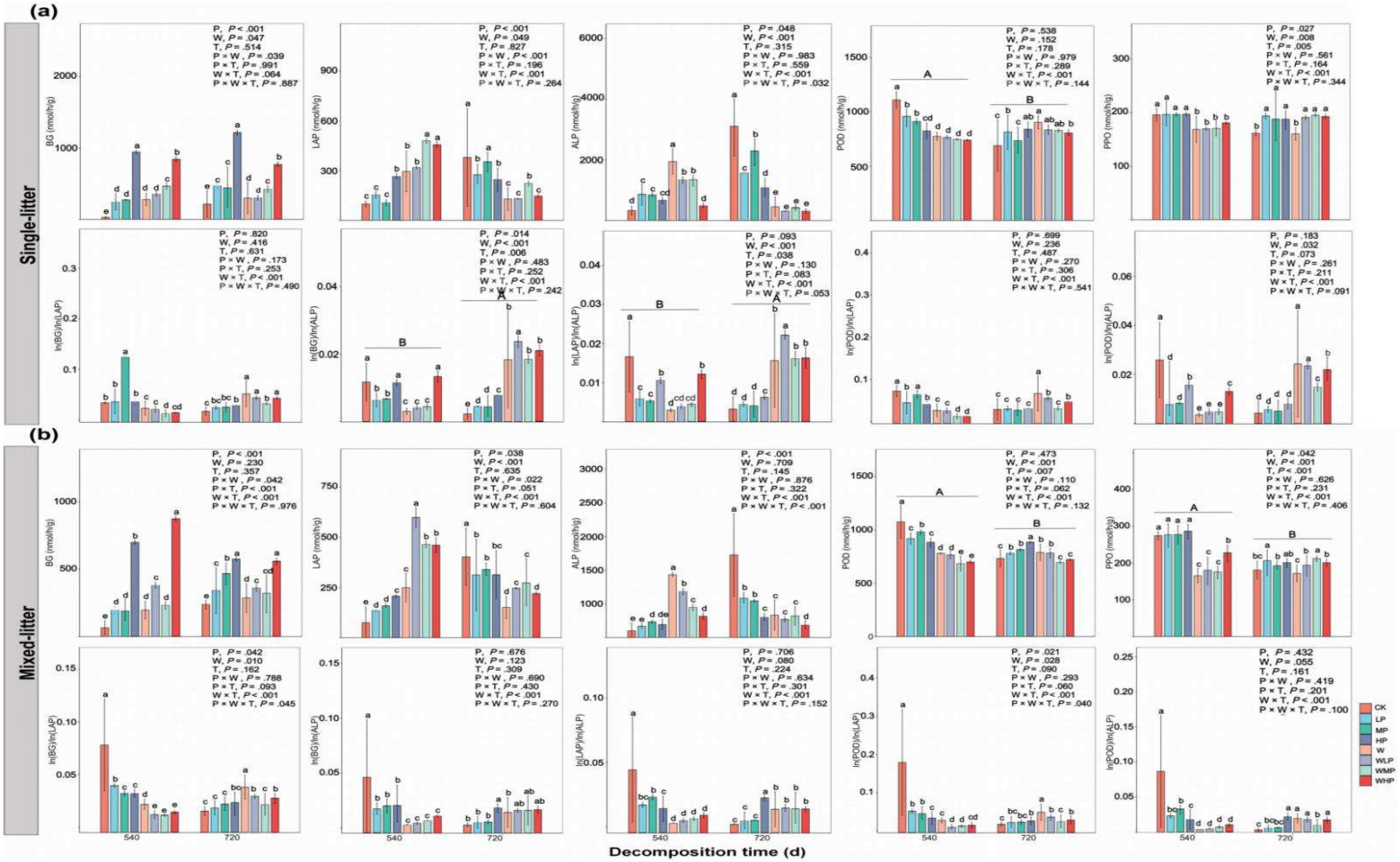


Fig. 3 Dynamics of soil extracellular enzyme activities and stoichiometric ratios of single-species (**a**) and mixed-species (**b**) litter. Different lowercase letters indicate significant differences among treatments at the same sampling time. Error bars represent standard error (n = 3, p < 0.05). Treatment descriptions are provided in Fig. 1.

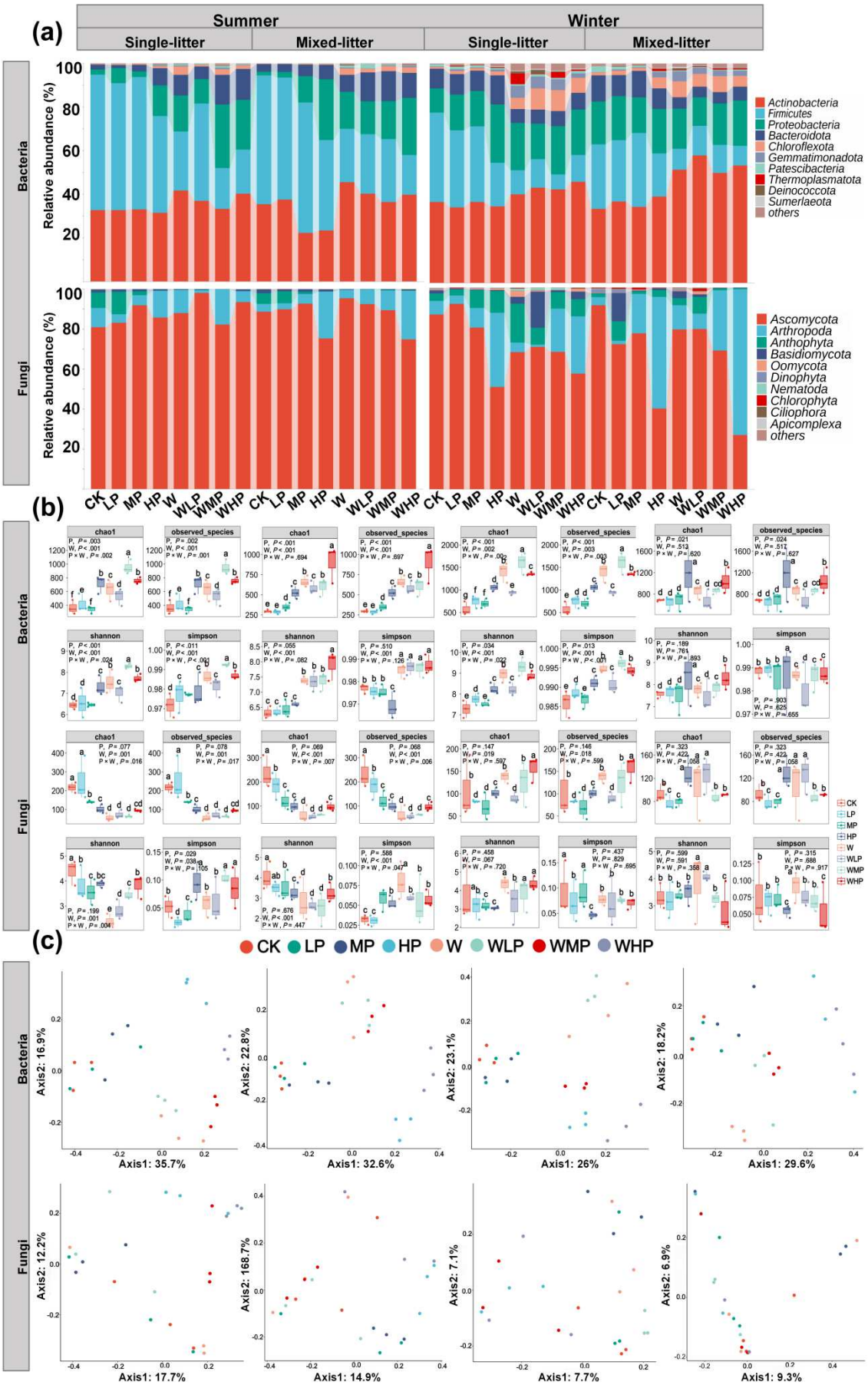

(a)
Summer
Winter
Single-litter
Mixed-litter
Single-litter
Mixed-litter
Bacteria
Fungi
Relative abundance (%)
Actinobacteria
Firmicutes
Proteobacteria
Bacteroidota
Chloroflexota
Gemmatimonadota
Patescibacteria
Thermoplasmatota
Deinococcota
Sumerlaeota
others
Ascomycota
Arthropoda
Anthophyta
Basidiomycota
Oomycota
Dinophyta
Nematoda
Chlorophyta
Ciliophora
Apicomplexa
others
CK LP MP HP W WLP WMP WHP
(b)
chao1
observed_species
shannon
simpson
(c)
CK LP MP HP W WLP WMP WHP
Axis1: 35.7%
Axis2: 16.9%
Axis1: 32.6%
Axis2: 22.8%
Axis1: 26%
Axis2: 23.1%
Axis1: 29.6%
Axis2: 18.2%
Axis1: 17.7%
Axis2: 12.2%
Axis1: 14.9%
Axis2: 168.7%
Axis1: 7.7%
Axis2: 7.1%
Axis1: 9.3%
Axis2: 6.9%

Fig. 4 Dynamics of soil microbial relative abundance at the phylum level (**a**), α-diversity (**b**), and *β*-diversity (**c**) in single- and mixed-species litter. Error bars represent standard error ($n = 3$, $p < 0.05$). The litter type and season labels at the top of panel (**a**) also apply to panels (**b**) and (**c**). Treatment descriptions are provided in Fig. 1.

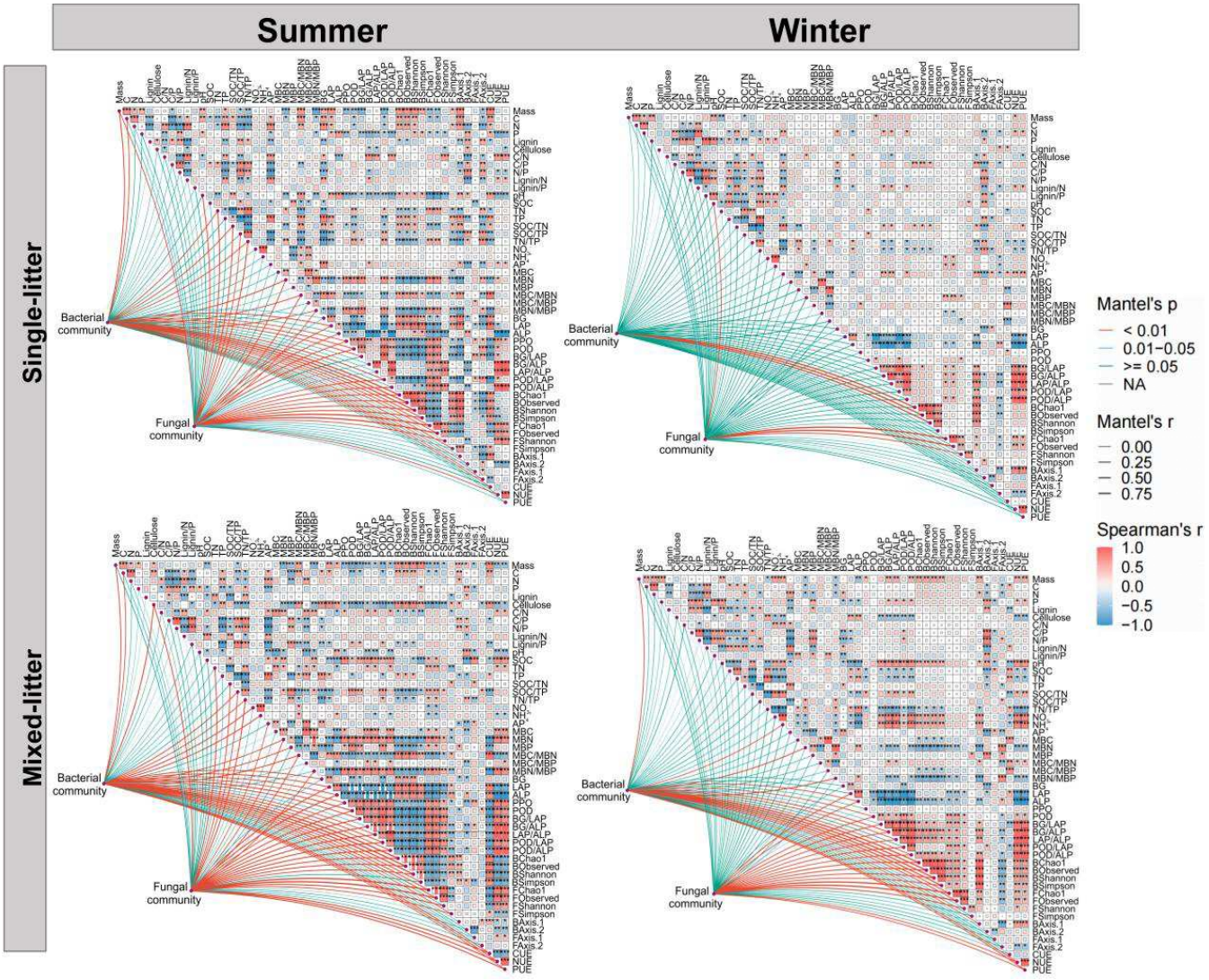


Fig. 5 Correlations between microbial communities and environmental factors across decomposition stages in single- and mixed-species litter. Mass: Mass loss; C: Carbon loss; N: N loss; P: P loss; Lignin: Lignin loss; Cellulose: Cellulose loss; SOC/TN: SOC/TN ratio; SOC/TP: SOC/TP ratio; TN/TP: TN/TP ratio; MBC/MBN: MBC/MBN ratio; MBC/MBP: MBC/MBP ratio; MBN/MBP: MBN/MBP ratio; BG/LAP: ln(BG)/ln(LAP) ratio; BG/ALP: ln(BG)/ln(ALP) ratio; LAP/ALP: ln(LAP)/ln(ALP) ratio; POD/LAP: ln(POD)/ln(LAP) ratio; POD/ALP: ln(POD)/ln(ALP) ratio; BChao1: Bacterial Chao1; BObserved: Bacterial Observed_species; BShannon: Bacterial Shannon; BSimpson: Bacterial Simpson; FChao1: Fungal Chao1; FObserved: Fungal Observed_species; FShannon: Fungal Shannon; FSimpson: Fungal Simpson ($n = 3$, ***$p < 0.001$, **$p < 0.01$, and *$p < 0.05$).

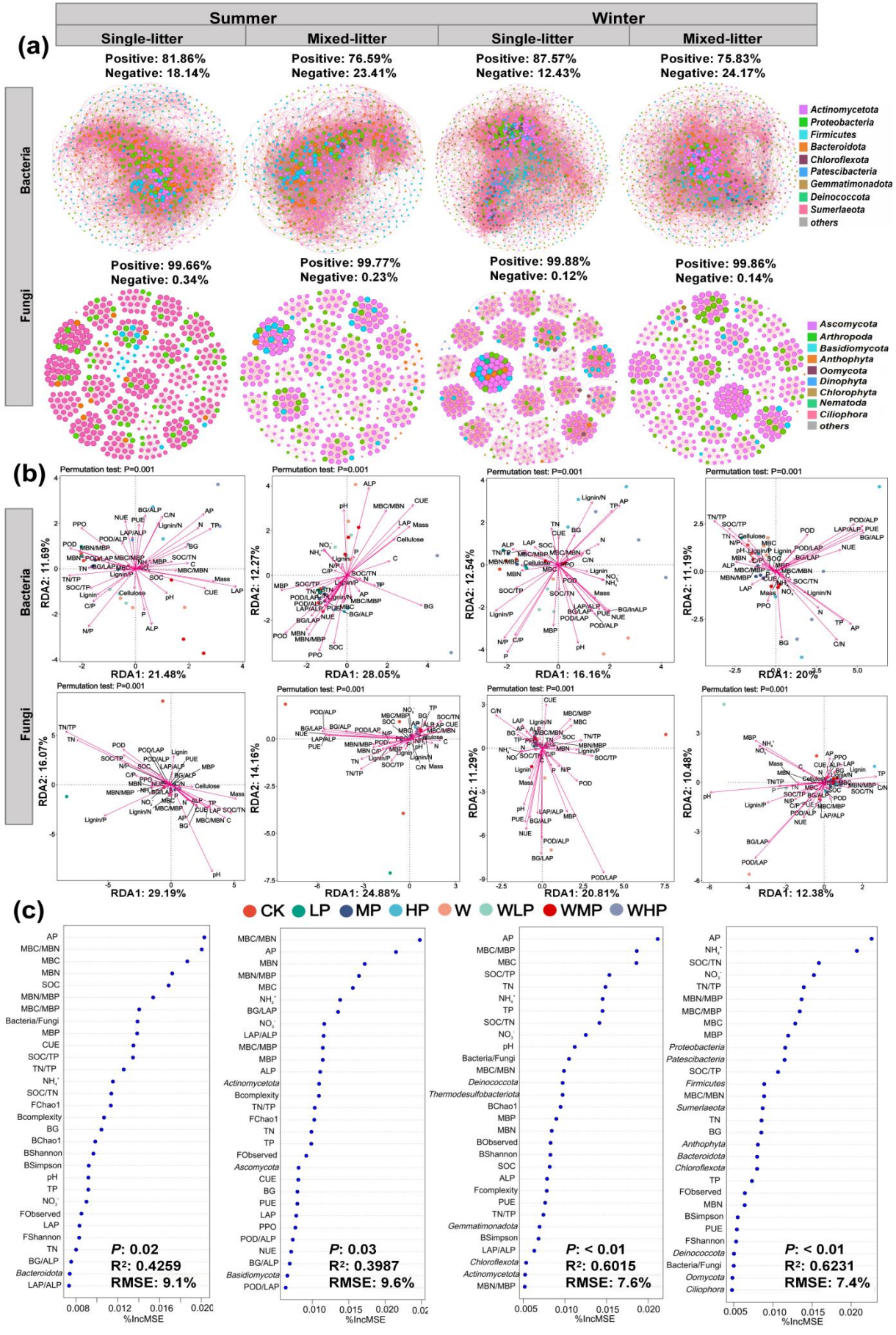

(a)
Summer
Winter
Single-litter
Mixed-litter
Single-litter
Mixed-litter
Positive: 81.86%
Negative: 18.14%
Positive: 76.59%
Negative: 23.41%
Positive: 87.57%
Negative: 12.43%
Positive: 75.83%
Negative: 24.17%
Bacteria
Fungi
Actinomycetota
Proteobacteria
Firmicutes
Bacteroidota
Chloroflexota
Patescibacteria
Gemmatimonadota
Deinococcota
Sumerlaeota
others
Positive: 99.66%
Negative: 0.34%
Positive: 99.77%
Negative: 0.23%
Positive: 99.88%
Negative: 0.12%
Positive: 99.86%
Negative: 0.14%
Ascomycota
Arthropoda
Basidiomycota
Anthophyta
Oomycota
Dinophyta
Chlorophyta
Nematoda
Ciliophora
others
(b)
Permutation test: P=0.001
RDA1: 21.48%
RDA2: 11.69%
RDA1: 28.05%
RDA2: 12.27%
RDA1: 16.16%
RDA2: 12.54%
RDA1: 20%
RDA2: 11.19%
RDA1: 29.19%
RDA2: 16.07%
RDA1: 24.88%
RDA2: 14.16%
RDA1: 20.81%
RDA2: 11.29%
RDA1: 12.38%
RDA2: 10.48%
(c)
CK
LP
MP
HP
W
WLP
WMP
WHP
P: 0.02
R²: 0.4259
RMSE: 9.1%
P: 0.03
R²: 0.3987
RMSE: 9.6%
P: < 0.01
R²: 0.6015
RMSE: 7.6%
P: < 0.01
R²: 0.6231
RMSE: 7.4%
%IncMSE

Fig. 6 Soil microbial co-occurrence networks (**a**), drivers and analysis of community structure (**b**), and evaluation of driver importance for litter decomposition (**c**) in single- and mixed-species litter. The bottom of the random forest model panels indicates the cross-validated R^2, root mean square error (RMSE), and the overall model significance *p*-value. The litter type and season labels at the top of panel (**a**) also apply to panels (**b**) and (**c**) ($p < 0.05$).

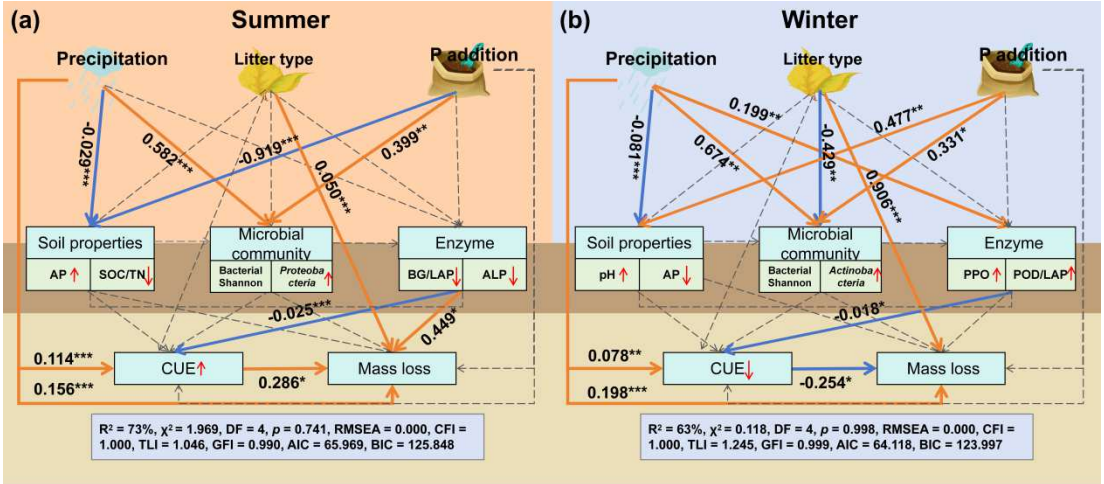


Fig. 7 Structural equation models (SEMs) of the key pathways controlling litter mass loss during summer (**a**) and winter (**b**). Values adjacent to arrows are standardized path coefficients. Orange and blue arrows denote positive and negative effects, respectively, while dashed arrows indicate non-significant relationships. R^2 values below each response variable represent the proportion of variance explained by the model. Significance levels: ***$p < 0.001$, **$p < 0.01$, and *$p < 0.05$.

Supplementary Files

This is a list of supplementary files associated with this preprint. Click to download.

- BFS.docx